# Unconditional Energy Stable Runge-Kutta Schemes for a Phase Field Model for Diblock Copolymers

Lizhen Chen and Bo Ren\*

Beijing Computational Science Research Center, Beijing 100193, P.R. China.

Received 3 August 2023; Accepted (in revised version) 22 October 2023.

**Abstract.** A high-accuracy and unconditional energy stable numerical scheme for a phase field model for diblock copolymers (PF-BCP model) is developed. The PF-BCP model is reformulated into an equivalent model, which based on scaler auxiliary variable (SAV) formulation. After that a stable Runge-Kutta (RK) method and a Fourier-spectral method are applied to the SAV-reformulated PF-BCP model to discretize on the temporal and spatial dimensions respectively. The fully discretized numerical scheme is computed by fixed-point iterations. Meanwhile, the unconditional energy decay property is proved rigorously. Finally, we present the results of numerical experiments to show the accuracy and efficiency of the RK scheme used and discuss the influence of physical parameters and initial conditions on the phase separation in the simulation of the PF-BCP model. In addition, the energy decay property of the numerical solutions is verified.

AMS subject classifications: 65M10, 78A48

Key words: Phase field model, diblock copolymer, auxiliary variable method, Runge-Kutta method.

#### 1. Introduction

The diblock copolymer model (DC model) is the system for a copolymer composed of two different monomers blocks A and B. The copolymer is formed by a linear-chain molecule of sub-chains of two different monomers blocks linked together at molecular scale characterized by fluid-like disorder. Due to incompatibility between two monomer blocks, they repulse each other, then tend to separate from mixture into pure blocks with free interfaces' occurring and deforming between two blocks. Finally, periodic structure is formed in diblock copolymer such as lamellar or cylindrical structures, which illustrates specific nano-materials.

To describe a complex system with fluid-like disorder composed of multiple components with free interfaces between them, we encounter challenges in matching boundary conditions on the interfaces in the Lagrangian framework. As a solution, the system is described

<sup>\*</sup>Corresponding author. Email addresses: lzchen@csrc.ac.cn (L. Chen), renbo\_mech@csrc.ac.cn (B. Ren)

by a phase field in the Eulerian framework, where the interface can be identified by field variable. The phase field model has been widely recognized as an effective approach to accurately depict such systems [6].

Firstly, we give some mathematical notions. For any functions f, g defined on a domain  $\Omega$ , we write

$$(f,g) := \int_{\Omega} f(\mathbf{x})g(\mathbf{x})d\mathbf{x}$$

for the  $L^2$  inner product of f, g. Besides, let  $||f|| := \sqrt{(f,f)}$  be the  $L^2$ -norm of f and

$$\bar{f} := \frac{1}{|\Omega|} \int_{\Omega} f(\mathbf{x}) d\mathbf{x}$$

the mean value of f.

The DC model is accurately described by the phase field for diblock copolymers (PF-BCP) in mean field theory. In the PF-BCP model, the phase field variable denoted by  $\phi(\mathbf{x},t)$  is introduced in the domain  $\Omega$ . This variable represents the difference in the fraction of mass between the two monomer blocks — i.e.  $N_A$  and  $N_B$  respectively denote the masses of monomer blocks A and B at the position  $\mathbf{x}$ , and the phase field variable  $\phi(\mathbf{x},t)$  is defined by

$$\phi(\mathbf{x},t) := (N_A - N_B)/(N_A + N_B).$$

The phase field  $\phi$  is a scalar variable representing the phase or state of the system. It takes values in the interval [-1,1]. The evolution of the PF-BCP model is to minimize the total free energy. The mixture state tends to separate and evolve into distinct pure A-monomer and pure B-monomer states with a specified infinitesimal interface between them. Over time, the PF-BCP system reaches a stable configuration where the separated phases coexist.

In the process of the DC model evolution, the total mass of the two monomers is conserved, resulting in the mass conservation property of the phase field. This can be expressed as

$$\frac{d}{dt} \int_{\Omega} \phi d\mathbf{x} = 0.$$

The evolution equation of the PF-BCP model is derived from the constrained gradient flow of the total free energy functional  $E(\phi)$  in the space  $H^{-1}$ , as described in [4]. The total free energy  $E(\phi)$  is a functional of the Cahn-Hilliard type energy endowed with an additional nonlocal term and is defined as

$$E(\phi) = \int_{\Omega} \left( \frac{\varepsilon^2}{2} |\nabla \phi|^2 + F(\phi) + \frac{\alpha}{2} |\nabla \psi|^2 \right) d\mathbf{x},$$

where

$$F(\phi) = \frac{(\phi^2 - 1)^2}{4}, \quad \psi = -\Delta^{-1}(\phi - \bar{\phi}).$$

In this expression, the term  $\varepsilon^2 |\nabla \phi|^2/2$  represents the interaction between the two monomer blocks,  $F(\phi)$  represents the potential energy density, and  $\alpha |\nabla \psi|^2/2$  represents the first-order effect of the connectivity between the two monomer blocks. Minimizing the functional  $E(\phi)$  by the constraint gradient flow method, we obtain the following evolution equation for the PF-BCP model:

$$\begin{split} \phi_t &= M \Delta \varphi & \text{in } \Omega \times [0, T], \\ \varphi &= -\varepsilon^2 \Delta \phi + f(\phi) + \alpha \psi & \text{in } \Omega \times [0, T], \\ -\Delta \psi &= \phi - \bar{\phi} & \text{in } \Omega \times [0, T], \\ \partial_{\mathbf{n}} \phi|_{\partial \Omega} &= \partial_{\mathbf{n}} \varphi|_{\partial \Omega} = \partial_{\mathbf{n}} \psi|_{\partial \Omega} = 0 & \text{or periodic boundary condition,} \end{split}$$
 (1.1)

where  $f(\phi) = F'(\phi)$ , M > 0 is a dimension of time or scaling on time, and  $\varepsilon > 0$  and  $\alpha > 0$  are model parameters that determine the fraction of different energy parts in the total free energy, and the mean mass is

$$\bar{\phi} = \frac{1}{|\Omega|} \int_{\Omega} \phi \, d\mathbf{x}.$$

The boundary conditions above are compatible with the mass conservation

$$\frac{d(\phi, 1)}{dt} = \int_{\Omega} M \Delta \varphi d\mathbf{x} = \int_{\partial \Omega} M \partial_{\mathbf{n}} \varphi ds = 0.$$

The evolution equation for the PF-BCP model is derived by minimizing the total free energy. Therefore, the PF-BCP model is dissipative with respect to the total free energy. We define the total free energy density as

$$E_{\rho} = \frac{\varepsilon^2}{2} |\nabla \phi|^2 + F(\phi) + \frac{\alpha}{2} |\nabla \psi|^2.$$

The energy dissipation rate can be calculated as follows:

$$\frac{dE}{dt} = \int_{\Omega} \frac{\delta E_{\rho}}{\delta \phi} \frac{\partial \phi}{\partial t} d\mathbf{x} = -\int_{\Omega} M |\nabla \varphi|^2 d\mathbf{x} \le 0.$$

The PF-BCP model provides quantitative description of evolution of mixture of two monomers in DC model, which can be used to study microscopic structures of nano-structured materials and nano-devices. Numerical computation of the PF-BCP model plays an important role in the study of the DC model. This is because the analytical solution of the equation is difficult to derive due to the complexity of the domain's geometry and the presence of a nonlinear term in PF-BCP model. Therefore, constructing efficient numerical schemes to the PF-BCP model become quite necessary, which may help study the evolution of the phase field. The efficiency of a numerical scheme for a model depends on its accuracy in approximating the exact solution. In the numerical computation of the phase field model, it is important for the numerical solution to preserve the dissipation property, which is an

intrinsic property of the phase field model. Note that any numerical solution preserving the dissipation property will be called the energy stable.

Constructing numerical schemes for the phase field models is significantly challenging, with the main difficulty being how to discretize the nonlinear term  $f(\phi)$  in evolution equations. In many phase field models, the nonlinear terms are complex and will cause stiffness at the interface between distinct phases, making it difficult to discretize them properly. Improper discretization of the nonlinear term may be result in unstable computations.

Previous research, including the works of [11,12], has focused on developing numerical schemes for the phase field model. However, these schemes have been limited to first-order accuracy and do not guarantee stability. Furthermore, the studies [3,8,15] show that using simple full-implicit or explicit discretization of the equations severely restricts the allowable temporal stepsize, particularly dependent on the interfacial width. To preserve the dissipation properties of the phase field model, several stable numerical schemes have been proposed based on convex splitting approaches or the linearization approach, as demonstrated in the works of [1,5,7,17]. However, these schemes are generally of low-accuracy order.

In our approach, instead of directly constructing numerical schemes for the phase field models, we utilize auxiliary variable methods to reformulate the models into equivalent forms by introducing additional variables. This allows us to construct numerical schemes for the reformulated models, which can provide stability and high accuracy. One popular approach for this is the invariant energy quadratization (IEQ) method, as demonstrated in works by [9, 18, 20]. The IEQ method aims to transform the total free energy density into a quadratic form involving both the phase variable and the introduced variable. The introduction of the new variable through the IEQ method provides more flexibility in constructing numerical schemes that satisfy efficiency requirements in numerical computation, including high-accuracy in and stability. The introduced variable in the IEQ method is defined as a function over the domain. However, the equivalent forms obtained through the IEQ method may lead to increased stiffness compared to the original phase field model after spatial discretization. To address this issue, the scalar auxiliary variable (SAV) method is introduced. The SAV method shares the same idea as the IEQ method by transforming the total free energy into a quadratic form, but it reformulates the phase field model into an equivalent form with an introduced scalar variable. Compared to the IEQ method, the SAV method retains almost all of its advantages and can be more efficient, as shown in works by [10, 13, 14, 19].

In this paper, we aim at constructing a high-accuracy and unconditional energy stable numerical scheme for the PF-BCP model. In Section 2, we introduce auxiliary variable methods to the general phase field model, which includes IEQ method and SAV method, then we reformulate SAV-reformulated PF-BCP model by SAV method. In Section 3, we introduce RK method for time-marching numerical computation, then apply the method to SAV-reformulated PF-BCP model to construct high-accuracy and energy stable numerical scheme. We prove our numerical scheme preserves mass conservation and energy decay. Furthermore, the fixed-point iteration is adopted to compute the nonlinear system. Finally, we apply Fourier-spectral method to discretize on the spatial dimension to obtain

full-discrete scheme. In Section 4, we present numerical experiments to show that our numerical scheme is highly-accurate and energy stable. We also study the effects of different initial conditions and varying parameters  $\alpha$  on phase separation's simulations of the PF-BCP model by our proposed algorithm.

# 2. Auxiliary Variable Methods for General Phase Field Model

In order to construct energy stable numerical scheme of high-accuracy for the phase field model, we introduce a new variable to reformulate the phase field model, which makes constructing numerical scheme such that all parts of total free energy synchronize more easily in numerical computation.

## 2.1. Gradient flow model as general phase field model

Most phase field models are derived from gradient flow of total free energy. We can regard the gradient flow model as general phase field model. The general phase field model consists of two key ingredients: the free energy density  $E_{\rho}$ , i.e.  $\int_{\Omega} E_{\rho} d\mathbf{x} = E$  and the kinetic equation dictated by a mobility matrix (or operator)  $\mathcal{G}$  in domain  $\Omega$ . We use  $\Phi = (\phi_1, \ldots, \phi_n)^T$  to denote the phase variable, we obtain the triple  $(\Phi, \mathcal{G}, E_{\rho})$  which defines a phase field model. The evolution equation in domain  $\Omega$  stemming from minimizing the total free energy, is given by

$$\partial_t \Phi(\mathbf{x}, t) = -\mathcal{G} \frac{\delta E_{\rho}}{\delta \Phi} \quad \text{in } \Omega,$$

$$\mathcal{C}(\Phi(\mathbf{x}, t)) = g(\mathbf{x}, t) \quad \text{on } \partial \Omega,$$
(2.1)

where  $\mathscr C$  is trace operator as boundary condition,  $\mathscr G=\mathscr G_a+\mathscr G_s$  is mobility operator decomposed as anti-symmetry and semi-positive definite parts. We call the variational derivation  $\delta E_\rho/\delta\Phi$  of  $E_\rho$  the chemical potential.

The general phase field model is derived through minimizing the total free energy by gradient flow method, the dissipation is intrinsic property of phase field model

$$\frac{dE}{dt} = \left(\frac{\delta E_{\rho}}{\delta \Phi}, \frac{\partial \Phi}{\partial t}\right) = \left(\frac{\delta E_{\rho}}{\delta \Phi}, -\mathcal{G}\frac{\delta E_{\rho}}{\delta \Phi}\right) = \left(\frac{\delta E_{\rho}}{\delta \Phi}, -\mathcal{G}_{s}\frac{\delta E_{\rho}}{\delta \Phi}\right) \leq 0.$$

As an example of the PF-BCP model (1.1), we take

$$E_{\rho} = \frac{\varepsilon^{2}}{2} |\nabla \phi|^{2} + F(\phi) + \frac{\alpha}{2} |\nabla \psi|^{2}, \mathcal{G} = -M\Delta$$

and the boundary condition of (1.1) as the trace operator, then the PF-BCP model has the form of (2.1).

# 2.2. Auxiliary variable methods to general phase field model

Generally the energy density of phase field model (2.1) has the form

$$E_{\rho} = \frac{1}{2} |\mathcal{L}^{1/2} \Phi|^2 + \mathcal{F}(\Phi),$$

where  $\mathcal{L}$  is linear (differential) operator and  $\mathcal{F}(\Phi)$  is functional of  $\Phi$ . The evolution equation of the phase field model is given by

$$\begin{split} \partial_t \Phi(\mathbf{x},t) &= -\mathcal{G}[\mathcal{L}\Phi + f(\Phi)] & \text{in } \Omega, \\ \mathcal{C}\big(\Phi(\mathbf{x},t)\big) &= g(\mathbf{x},t) & \text{on } \partial\Omega, \end{split}$$

where  $f(\Phi) = \mathscr{F}'(\Phi)$ . When f is nonlinear functional, it prevents the design of efficient numerical methods to the phase field model. We apply auxiliary variable method to phase field model to transform it into equivalent reformation with auxiliary variable. There are two auxiliary variable methods used popularly in phase field model, IEQ method and SAV method.

Introducing variable  $R = \sqrt{\int_{\Omega} 2\mathscr{F}(\Phi) d\mathbf{x}}$ , we write the total free energy as

$$E(\Phi,R) = \frac{1}{2}(\mathcal{L}\Phi,\Phi) + \frac{1}{2}|R|^2.$$

With the introduced variable, we can reformulate the phase field model into one equivalent model called SAV-reformulated phase field model

$$\begin{split} \partial_t \Phi &= -\mathcal{G} \left[ \mathcal{L} \Phi + RW(\Phi) \right] & \text{in } \Omega, \\ \partial_t R &= \left( W(\Phi), \partial_t \Phi \right) & \text{in } \Omega, \\ C(\Phi) &= g(\mathbf{x}, t) & \text{on } \partial \Omega, \end{split}$$
 (2.2)

where

$$W(\Phi) = f(\Phi)/\sqrt{\int_{\Omega} 2\mathscr{F}(\Phi)d\mathbf{x}}.$$

The initial condition is given by

$$\Phi|_{t=0} = \Phi^0, \quad R|_{t=0} = \sqrt{\int_{\Omega} 2\mathscr{F}(\Phi^0) d\mathbf{x}}.$$

In order to construct efficient numerical schemes for general phase field model (2.1), we can design a numerical scheme for (2.3) or (2.2) instead of (2.1), which can help with constructing numerical schemes that synchronize all parts of total free energy to preserve energy decay. Auxiliary variable can be viewed as a new freedom for constructing numerical schemes, we can have more ways to construct numerical schemes to satisfy what we require. What is more, the nonlinear term  $f(\Phi)$  is converted into multiplication of two variables instead of a complex functional of variable  $\Phi$  by using auxiliary variable method, thus the energy stable linearized numerical scheme's construction can be easier.

There is another auxiliary variable method used popularly in phase field model, IEQ method, is described as follows.

**Remark 2.1.** We illustrate the ideal by transforming the free energy density  $E_{\rho}$  into a quadratic one, the introduced auxiliary variable Q is obtained as removing the quadratic gradient term  $|\mathcal{L}^{1/2}\Phi|^2/2$  from the energy density

$$Q = \sqrt{2\bigg(E_\rho - \frac{1}{2}|\mathcal{L}^{1/2}\Phi|^2\bigg)} = \sqrt{2\mathscr{F}(\Phi)}.$$

The total free energy is rewritten as

$$E(\Phi, Q) = \left(\frac{1}{2}\Phi, \mathcal{L}\Phi\right) + \left(\frac{1}{2}Q, Q\right),$$

and the energy density is rewritten as

$$E_{\rho}(\Phi, Q) = \frac{1}{2} |\mathcal{L}^{1/2}\Phi|^2 + \frac{1}{2} |Q|^2,$$

where *Q* is a function of variables  $\Phi$ , i.e.  $Q = Q(\Phi)$ . Denoting

$$H(\Phi) = \frac{f(\Phi)}{\sqrt{2\mathscr{F}(\Phi)}} = \frac{\delta Q}{\delta \Phi},$$

we can reformulate the model (2.1) into an equivalent form — viz.

$$\begin{split} \partial_t \Phi &= -\mathcal{G} \left[ \mathcal{L} \Phi + Q H(\Phi) \right] & \text{in } \Omega, \\ \partial_t Q &= H(\Phi) : \partial_t \Phi & \text{in } \Omega, \\ C(\Phi) &= g(\mathbf{x}, t) & \text{on } \partial \Omega. \end{split} \tag{2.3}$$

The initial condition is given by

$$\Phi|_{t=0} = \Phi^0, \quad Q|_{t=0} = \sqrt{2\mathscr{F}(\Phi^0)}.$$

**Remark 2.2.** We always assume that  $\mathscr{F}(\Phi) > 0$ . Otherwise, we let  $\mathscr{F}(\Phi) := \mathscr{F}(\Phi) + A_0 \ge 0$ , so that it is a well-defined real variable.

## 2.3. Reformulated PF-BCP models by auxiliary variable methods

Applying SAV method to PF-BCP model (1.1), we can obtain equivalent reformulated form of PF-BCP model.

For SAV-reformulated PF-BCP model, we introduce  $r = \sqrt{\int_{\Omega} 2F(\phi)d\mathbf{x}}$ , so that the total free energy is transformed into

$$E(\phi, r) = \frac{\varepsilon^2}{2} \|\nabla \phi\|^2 + \frac{1}{2} |r|^2 + \frac{\alpha}{2} \|\nabla \psi\|^2$$

and the evolution equations are rewritten as

$$\begin{split} \phi_t &= M \Delta \varphi & \text{in } \Omega, \\ \varphi &= -\varepsilon^2 \Delta \phi + r w(\phi) + \alpha \psi & \text{in } \Omega, \\ -\Delta \psi &= \phi - \bar{\phi} & \text{in } \Omega, \\ r_t &= \left( w(\phi), \phi_t \right) & \text{in } \Omega, \\ \partial_n \phi &= \partial_n \varphi = \partial_n \psi = 0 & \text{or periodic on } \partial \Omega, \end{split}$$
 (2.4)

where

$$w(\phi) = f(\phi)/\sqrt{\int_{\Omega} 2F(\phi)d\mathbf{x}}.$$

The initial condition is given by

$$|\phi|_{t=0} = \phi^0, \quad r|_{t=0} = \sqrt{\int_{\Omega} 2F(\phi^0) d\mathbf{x}}.$$

Remark 2.3. For IEQ-reformulated PF-BCP model, we introduce the variable

$$q = \sqrt{2\left(E_{\rho} - \frac{\varepsilon^2}{2}|\nabla\phi|^2 - \frac{\alpha}{2}|\nabla\psi|^2\right)} = \sqrt{2F(\phi)}$$

and write the total free energy density as

$$E_{\rho} = \frac{\varepsilon^2}{2} |\nabla \phi|^2 + \frac{1}{2} |q|^2 + \frac{\alpha}{2} |\nabla \psi|,$$

and the evolution equations as

$$\begin{split} \phi_t &= M \Delta \varphi & \text{in } \Omega, \\ \varphi &= -\varepsilon^2 \Delta \phi + q h(\phi) + \alpha \psi & \text{in } \Omega, \\ -\Delta \psi &= \phi - \bar{\phi} & \text{in } \Omega, \\ q_t &= h(\phi) \phi_t & \text{in } \Omega, \\ \partial_{\mathbf{n}} \phi &= \partial_{\mathbf{n}} \varphi = \partial_{\mathbf{n}} \psi = 0 & \text{or periodic on } \partial \Omega, \end{split}$$

where

$$h(\phi) = \frac{f(\phi)}{\sqrt{2F(\phi)}} = \frac{\delta q}{\delta \phi}.$$

The initial condition is given by

$$\phi|_{t=0} = \phi^0$$
,  $q|_{t=0} = \sqrt{2F(\phi^0)}$ .

# 3. Algebraically Stable Runge-Kutta Scheme

In this section, we adopt algebraically stable Runge-Kutta (RK) method to construct energy stable and highly-accurate time-marching numerical scheme for SAV-reformulated PF-BCP model (2.4). Then for spatial dimension, we apply Fourier spectral method to obtain the full-discrete scheme.

## 3.1. Algebraically stable Runge-Kutta method

The RK method, as a high-accuracy numerical method, is widely used in numerical time-marching computation for differential equations. In the process of the RK method, we first separate temporal interval [0,T] uniformly with stepsize  $\tau>0$  to obtain the temporal nodes  $0=t_0< t_1< \cdots < t_{N-1}< t_N=T$  where  $t_{n+1}-t_n=\tau$  for  $0\leq n\leq N-1$ , with given coefficients of s-stage RK method in following so-called Butcher Tableau:

Table 1: Butcher Tableau.

We compute the following differential system, which is the form of (2.4):

$$\dot{y} = f(y), \quad y|_{t=0} = y^0.$$

For given  $y^n$  at  $t = t_n$ , one computes  $y^{n+1}$  by

$$y^{ni} = y^n + \tau \sum_{j=1}^s a_{ij} \dot{y}^{nj}, \quad i = 1, ..., s,$$
  
 $y^{n+1} = y^n + \tau \sum_{i=1}^s b_i \dot{y}^{ni}.$ 

Here for brevity we take notion  $t_{ni} = t_n + c_i \tau$ , i = 1,...,s and  $y^{ni}$  is approximation to  $y(t_{ni})$  for i = 1,...,s.

The coefficients in Butcher Tableau determine the efficiency of RK method, which includes accuracy and stability. Generally these coefficients have consistency conditions

$$\sum_{i=1}^{s} b_i = 1, \quad \sum_{i=1}^{s} a_{ki} = c_k, \quad k = 1, \dots, s.$$

**Stability condition.** We consider RK method whose coefficients satisfy the following conditions:

- The matrix  $A = (a_{ij})_{s \times s}$  is invertible.
- $b_i > 0$ , i = 1, ..., q.
- $c_i \neq c_j$  for  $i \neq j$ .
- The matrix  $M = (m_{ij})_{s \times s}$  with entries  $m_{ij} = b_i a_{ij} + b_j a_{ji} b_i b_j$  is symmetric positive semi-definite.

Any RK method satisfying these stability conditions is called algebraically stable.

**Accuracy conditions.** We also assume that the algebraically stable RK method is associated with a collocation method — i.e. the parameters in Butcher Tableau  $c_i$ , i = 1, ..., s are chosen from some special polynomial's (such as shifted Legendre polynomial) zeros in interval [0,1],

$$a_{ij} = \int_0^{c_i} l_j(t)dt, \quad b_i = \int_0^1 l_i(t)dt,$$

where

$$l_i(t) = \Pi_{j \neq i} \frac{t - c_j}{c_i - c_j}, \quad 1 \le i \le s$$

are the Lagrangian polynomials based on the zeros  $c_i$ ,  $1 \le i \le s$ . We assume that the coefficients of RK method in Butcher Tableau satisfy the following accuracy assumptions:

$$\sum_{i=1}^{s} b_i c_i^{l-1} = \frac{1}{l}, \qquad l = 1, \dots, p,$$
(3.1)

$$\sum_{i=1}^{s} a_{ij} c_j^{l-1} = \frac{c_i^{l-1}}{l}, \qquad l = 1, \dots, q_1, \quad i = 1, \dots, s,$$
(3.2)

$$\sum_{j=1}^{s} a_{ij} b_i c_j^{l-1} = \frac{c_i^{l-1}}{l}, \quad l = 1, \dots, q_2, \quad i = 1, \dots, s.$$
 (3.3)

There are two popular families of Runge-Kutta methods of collocation type satisfying the stability and accuracy conditions — viz. Gauss method and Radau IIA method [16]. For accuracy, they have conditions p=2s and p=2s-1 in condition (3.1) respectively,  $q_1=s$  in condition (3.2), then  $q_2=s,s-1$  in condition (3.3) respectively, the detail can refer to [16, Chapter IV, Lemma 5.4]. Here we have the following theorem of accuracy for RK methods under the above assumptions.

**Theorem 3.1** (cf. Wanner & Hairer [16, Chapter IV, Theorem 5.1]). If the coefficients  $b_i$ ,  $c_i$ ,  $a_{ij}$  of the RK method satisfy conditions (3.1)-(3.3), where  $p \le q_1+q_2+1$  and  $p \le 2q_1+2$ , then the RK method is time-marching numerical method of order p.

The convergence order for the Gauss method and Rudua IIA methods can refer to the following theorem.

**Theorem 3.2.** With the assumption of  $p,q_1,q_2$ , s-stage Gauss and Radua IIA method are time-marching numerical method of convergence order 2s and order 2s - 1 respectively.

For Gauss method and Rudua IIA method, arbitrary high-order method can be constructed [16].

## 3.2. Time-marching numerical scheme

We apply algebraically stable RK methods to SAV-reformulated PF-BCP model (2.4) to construct numerical scheme to compute  $\phi^{n+1}$  and  $r^{n+1}$  at  $t=t_{n+1}$  with given  $\phi^n$  and  $r^n$  at  $t=t_n$ . First we compute internal values  $(\phi^{ni}, r^{ni})$ ,  $i=1,\ldots,s$  by solving

$$\dot{\phi}^{ni} = M\Delta\varphi^{ni} \qquad \text{in } \Omega, \quad i = 1, \dots, s,$$

$$\phi^{ni} = \phi^n + \tau \sum_{j=1}^s a_{ij} \dot{\phi}^{nj} \qquad \text{in } \Omega, \quad i = 1, \dots, s,$$

$$\varphi^{ni} = -\varepsilon^2 \Delta \phi^{ni} + r^{ni} w(\phi^{ni}) + \alpha \psi^{ni} \qquad \text{in } \Omega, \quad i = 1, \dots, s,$$

$$-\Delta \psi^{ni} = \phi^{ni} - \bar{\phi}^{ni} \qquad \text{in } \Omega, \quad i = 1, \dots, s,$$

$$\partial_n \phi^{ni} = \partial_n \varphi^{ni} = \partial_n \psi^{ni} = 0 \qquad \text{or periodic on } \partial \Omega, \quad i = 1, \dots, s,$$

$$\dot{r}^{ni} = \left(w(\phi^{ni}), \dot{\phi}^{ni}\right), \quad i = 1, \dots, s,$$

$$r^{ni} = r^n + \tau \sum_{i=1}^s a_{ij} \dot{r}^{ni}, \quad i = 1, \dots, s,$$

$$(3.5)$$

which is a differential system of  $(\phi^{ni}, r^{ni})$ , i = 1, ..., s, we can obtain  $(\phi^{ni}, r^{ni})$ , i = 1, ..., s by solving this differential system. Then we can obtain unique  $(\dot{\phi}^{ni}, \dot{r}^{ni})$  by both second relations of (3.4) and (3.5) due to the invertibility of matrix  $A = (a_{ij})_{s \times s}$ . Using  $(\dot{\phi}^{ni}, \dot{r}^{ni})$  we compute

$$\phi^{n+1} = \phi^n + \tau \sum_{i=1}^s b_i \dot{\phi}^{ni},$$

$$r^{n+1} = r^n + \tau \sum_{i=1}^s b_i \dot{r}^{ni}.$$
(3.6)

# 3.3. Mass conservation and energy dissipation of time discretized scheme

In this section, we present some properties of the numerical scheme (3.4)-(3.6) that the mass  $\int_{\Omega} \phi^n d\mathbf{x}$  is conservative and the discrete energy is decayed — i.e. our time-marching scheme preserves the mass conservation and dissipation properties of the PF-BCP model.

#### 3.3.1. Mass conservation

Firstly, we check that the numerical scheme (3.4)-(3.6) has the mass conservation property as follows.

**Theorem 3.3** (Mass Conservation). For given initial condition  $\phi(\cdot,0) = \phi^0$ , we compute the numerical scheme (3.4)-(3.6) to obtain  $\phi^{ni}$ ,  $i=1,\ldots,s$  and  $\phi^{n+1}$  which denote the numerical approximations of  $\phi$  at  $t=t_{ni}$  and  $t=t_{n+1}$ , respectively. Then the mass  $\int_{\Omega} \phi^{n+1} d\mathbf{x}$  and mass  $\int_{\Omega} \phi^{ni} d\mathbf{x}$  preserve constant — i.e.

$$\int_{\Omega} \phi^{ni} d\mathbf{x} = \int_{\Omega} \phi^{n+1} d\mathbf{x} = \int_{\Omega} \phi^{0} d\mathbf{x}, \quad n = 0, 1, \dots, N-1.$$

*Proof.* We take  $L^2$  inner product of the first relation of (3.4) with the identity function 1. Using the boundary condition of (3.4) gives

$$\int_{\Omega} \dot{\phi}^{ni} d\mathbf{x} = (\dot{\phi}^{ni}, 1) = M \int_{\Omega} \Delta \varphi^{ni} d\mathbf{x} = M \int_{\partial \Omega} \nabla \varphi^{ni} \cdot \mathbf{n} dS = M \int_{\partial \Omega} \partial_{\mathbf{n}} \varphi^{ni} dS = 0.$$

With the above result, we then take the  $L^2$  inner product with 1 of the first relation of (3.6), we have

$$\int_{\Omega} \phi^{n+1} d\mathbf{x} = (\phi^{n+1}, 1) = (\phi^{n}, 1) + \int_{\Omega} \tau \sum_{i=1}^{s} b_{i} \dot{\phi}^{ni} d\mathbf{x}$$
$$= \int_{\Omega} \phi^{n} d\mathbf{x} + \tau \sum_{i=1}^{s} b_{i} \int_{\Omega} \dot{\phi}^{ni} d\mathbf{x} = \int_{\Omega} \phi^{n} d\mathbf{x}.$$

Setting n = 0, we can obtain the results for n = 1, ..., N - 1, hence we have

$$\int_{\Omega} \phi^{n+1} d\mathbf{x} = \int_{\Omega} \phi^0 d\mathbf{x}, \quad 0 \le n \le N-1.$$

Similarly, take the inner product of the second relation of (3.4), we obtain the mass conservation at internal stages,

$$\int_{\Omega} \phi^{ni} d\mathbf{x} = \int_{\Omega} \phi^{0} d\mathbf{x}, \quad 0 \le n \le N - 1, \quad i = 1, \dots, s.$$

## 3.3.2. Discrete energy decay

The energy decay (dissipation) is an intrinsic property of phase field models. In this subsection, we verify the energy decay for the numerical scheme (3.4)-(3.6) in the sense of the defined energy

$$E(\phi^{n}, r^{n}) = \frac{\varepsilon^{2}}{2} \|\nabla \phi^{n}\|^{2} + \frac{1}{2} |r^{n}|^{2} + \frac{\alpha}{2} \|\nabla \psi^{n}\|^{2}.$$

**Theorem 3.4** (Discrete Energy Decay). Assume that the RK method is algebraically stable with given initial values  $(\phi^n, r^n) \in H^1(\Omega) \times \mathbb{R}$ . Then the numerical scheme (3.4)-(3.5) has numerical solution on the internal nodes  $(\phi^{ni}, r^{ni}) \in H^1(\Omega) \times \mathbb{R}$ , and the nodal values  $(\phi^{n+1}, r^{n+1}) \in H^1(\Omega) \times \mathbb{R}$  defined by (3.6) satisfies the energy decay

$$E(\phi^{n+1},r^{n+1}) \leq E(\phi^n,r^n).$$

*Proof.* For the first term  $\|\nabla \phi^{n+1}\|^2$ , in terms of the first relation in (3.6), by taking  $\nabla$  on both sides we have

$$\nabla \phi^{n+1} = \nabla \phi^n + \tau \sum_{i=1}^s b_i \nabla \dot{\phi}^{ni},$$

then square of  $L^2$ -norms of both sides to get

$$\begin{split} \|\nabla\phi^{n+1}\|^2 &= \left(\nabla\phi^{n} + \tau \sum_{i=1}^{s} b_{i} \nabla\dot{\phi}^{ni}, \nabla\phi^{n} + \tau \sum_{i=1}^{s} b_{i} \nabla\dot{\phi}^{ni}\right) \\ &= \|\nabla\phi^{n}\|^{2} + 2\tau \sum_{i=1}^{s} b_{i} (\nabla\dot{\phi}^{ni}, \nabla\phi^{n}) + \tau^{2} \sum_{i,i=1}^{s} b_{i} b_{j} (\nabla\dot{\phi}^{ni}, \nabla\dot{\phi}^{nj}). \end{split}$$

Substituting

$$\phi^n = \phi^{ni} - \tau \sum_{i=1}^s a_{ij} \dot{\phi}^{ni}$$

from (3.4) into the second term yields

$$\begin{split} \|\nabla\phi^{n+1}\|^2 &= \|\nabla\phi^n\|^2 + 2\tau \sum_{i=1}^s b_i \Bigg(\nabla\dot\phi^{ni}, \nabla\phi^{ni} - \tau \sum_{j=1}^s a_{ij}\nabla\dot\phi^{nj}\Bigg) \\ &+ \tau^2 \sum_{i,j=1}^s b_i b_j (\nabla\dot\phi^{ni}, \nabla\dot\phi^{nj}). \end{split}$$

Then we obtain

$$\|\nabla \phi^{n+1}\|^2 = \|\nabla \phi^n\|^2 + 2\tau \sum_{i=1}^s b_i (\nabla \dot{\phi}^{ni}, \nabla \phi^{ni}) - \tau^2 \sum_{i,j=1}^s m_{ij} (\nabla \dot{\phi}^{ni}, \nabla \dot{\phi}^{nj})$$

with

$$m_{ij} = b_j a_{ij} + b_j a_{ji} - b_i b_j, \quad i, j = 1, ..., s.$$

Due to the positive semi-definiteness of  $(m_{ij})_{s\times s}$ , we can infer that

$$\|\nabla \phi^{n+1}\|^2 \le \|\nabla \phi^n\|^2 + 2\tau \sum_{i=1}^s b_i(\nabla \dot{\phi}^{ni}, \nabla \phi^{ni}). \tag{3.7}$$

We test the first relation of (3.4) with  $\varphi^{ni}$ , so that

$$(\dot{\varphi}^{ni},\varphi^{ni})=M(\Delta\varphi^{ni},\varphi^{ni})=-M(\nabla\varphi^{ni},\nabla\varphi^{ni}).$$

Substituting the third relation

$$\varphi^{ni} = -\varepsilon^2 \Delta \phi^{ni} + r^{ni} w(\phi^{ni}) + \alpha \psi^{ni}$$

from (3.4) into the first inner product gives

$$\begin{split} -M\|\nabla\varphi^{ni}\|^2 &= \left(\dot{\varphi}^{ni}, -\varepsilon^2\Delta\varphi^{ni} + r^{ni}w(\varphi^{ni}) + \alpha\psi^{ni}\right) \\ &= \varepsilon^2(\nabla\dot{\varphi}^{ni}, \nabla\varphi^{ni}) + \left(\dot{\varphi}^{ni}, r^{ni}w(\varphi^{ni}) + \alpha\psi^{ni}\right). \end{split}$$

We can infer that

$$\varepsilon^{2}(\nabla \dot{\phi}^{ni}, \nabla \phi^{ni}) = -(\dot{\phi}^{ni}, r^{ni}w(\phi^{ni}) + \alpha \psi^{ni}) - M \|\nabla \varphi^{ni}\|^{2}.$$

Substituting this relation into (3.7), we get

$$\begin{split} \|\nabla \phi^{n+1}\|^{2} &\leq \|\nabla \phi^{n}\|^{2} + \frac{2\tau}{\varepsilon^{2}} \sum_{i=1}^{s} b_{i} \left[ -(\dot{\phi}^{ni}, r^{ni}w(\phi^{ni}) + \alpha \psi^{ni}) - M \|\nabla \varphi^{ni}\|^{2} \right] \\ &\leq \|\nabla \phi^{n}\|^{2} + \frac{2\tau}{\varepsilon^{2}} \sum_{i=1}^{s} b_{i} \left[ -(\dot{\phi}^{ni}, r^{ni}w(\phi^{ni}) + \alpha \psi^{ni}) \right]. \end{split}$$

We now analyse the term  $|r^{n+1}|^2$  similarly. Squaring of both sides of the second relation of (3.6) yields

$$|r^{n+1}|^2 = |r^n|^2 + 2\tau \sum_{i=1}^s b_i r^n \dot{r}^{ni} + \tau^2 \sum_{i,j=1}^s b_i b_j |\dot{r}^{ni}|^2.$$

Substituting  $r^n = r^{ni} - \tau \sum_{j=1}^s a_{ij} r^{nj}$  into the second term of the right side in above quality yields

$$|r^{n+1}|^2 = |r^n|^2 + 2\tau \sum_{i=1}^s b_i \left( r^{ni} - \tau \sum_{j=1}^s a_{ij} r^{nj} \right) \dot{r}^{ni} + \tau^2 \sum_{i,j=1}^s b_i b_j |\dot{r}^{ni}|^2.$$

Therefore,

$$|r^{n+1}|^2 = |r^n|^2 + 2\tau \sum_{i=1}^s b_i r^{ni} \dot{r}^{ni} - \tau^2 \sum_{i,j=1}^s m_{ij} |\dot{r}^{ni}|^2$$

with

$$m_{ij} = b_i a_{ij} + b_j a_{ji} - b_i b_j, \quad i, j = 1, ..., s.$$

Due to the positive semi-definiteness of  $(m_{ij})_{s \times s}$ , we have

$$|r^{n+1}|^2 \le |r^n|^2 + 2\tau \sum_{i=1}^s b_i r^{ni} \dot{r}^{ni}. \tag{3.8}$$

With the expressions (3.5), we have

$$r^{ni}\dot{r}^{ni} = (r^{ni}w(\phi^{ni}), \dot{\phi}^{ni}).$$

Substituting this into (3.8) yields

$$|r^{n+1}|^2 \le |r^n|^2 + 2\tau \sum_{i=1}^s b_i (r^{ni}w(\phi^{ni}), \dot{\phi}^{ni}).$$

Multiplying  $\|\nabla \phi^{n+1}\|^2$  and  $|r^{n+1}|$  respectively by  $\varepsilon^2/2$  and 1/2 and summing these two terms, we obtain

$$\frac{\varepsilon^{2}}{2} \|\nabla \phi^{n+1}\|^{2} + \frac{1}{2} |r^{n+1}|^{2}$$

$$\leq \frac{\varepsilon^{2}}{2} \|\nabla \phi^{n}\|^{2} + \frac{1}{2} |r^{n}|^{2} + \tau \sum_{i=1}^{s} b_{i} \left[ -(\dot{\phi}^{ni}, r^{ni} w(\phi^{ni}) + \alpha \psi^{ni}) \right]$$

$$+ \tau \sum_{i=1}^{s} b_{i} \left( r^{ni} w(\phi^{ni}), \dot{\phi}^{ni} \right)$$

$$= \frac{\varepsilon^{2}}{2} \|\nabla \phi^{n}\|^{2} + \frac{1}{2} |r^{n}|^{2} - \tau \sum_{i=1}^{s} b_{i} (\dot{\phi}^{ni}, \alpha \psi^{ni}).$$
(3.9)

The remaining part is to prove

$$\tau \sum_{i=1}^{s} b_i(\dot{\phi}^{ni}, \alpha \psi^{ni}) \ge \frac{\alpha}{2} (\|\nabla \psi^{n+1}\|^2 - \|\nabla \psi^n\|^2).$$

With the forth relation in (3.4) and the mass conservation — i.e.  $\bar{\phi}^{ni}$  is constant, we have

$$\begin{split} (\dot{\phi}^{ni}, \alpha \psi^{ni}) &= \alpha (\dot{\phi}^{ni} - \dot{\bar{\phi}}^{ni}, \psi^{ni}) + \alpha (\dot{\bar{\phi}}^{ni}, \psi^{ni}) \\ &= -\alpha (\Delta \dot{\psi}^{ni}, \psi^{ni}) + \alpha (\dot{\bar{\phi}}^{ni}, \psi^{ni}) \\ &= \alpha (\nabla \dot{\psi}^{ni}, \nabla \psi^{ni}) + \alpha (\dot{\bar{\phi}}^{ni}, \psi^{ni}) \\ &= \alpha (\nabla \dot{\psi}^{ni}, \nabla \psi^{ni}) + \frac{\alpha}{|\Omega|} (\dot{\phi}^{ni}, 1) (1, \psi^{ni}) \\ &= \alpha (\nabla \dot{\psi}^{ni}, \nabla \psi^{ni}). \end{split}$$

Here  $\dot{\bar{\phi}}^{ni}=0$  is defined by the approximation of  $\bar{\phi}_t(\cdot,t_{ni})=0$  and the expression  $\Delta\dot{\psi}^{ni}=\dot{\phi}^{ni}-\dot{\bar{\phi}}^{ni}$  is defined by the forth relation of (3.4).

Since

$$\phi^{n+1} = \phi^n + \tau \sum_{i=1}^s b_i \dot{\phi}^{ni},$$

$$\phi^{ni} = \phi^n + \tau \sum_{j=1}^s a_{ij} \dot{\phi}^{nj},$$

$$\bar{\phi}^{n+1} = \bar{\phi}^n = \bar{\phi}^{ni}, \quad \dot{\bar{\phi}}^{ni} = 0,$$

we have

$$\phi^{n+1} - \bar{\phi}^{n+1} = \phi^n - \bar{\phi}^n + \tau \sum_{i=1}^s b_i (\dot{\phi}^{ni} - \dot{\bar{\phi}}^{ni}),$$

$$\phi^{ni} - \bar{\phi}^{ni} = \phi^n - \bar{\phi}^n + \tau \sum_{i=1}^s a_{ij} (\dot{\phi}^{nj} - \dot{\bar{\phi}}^{nj}).$$

Taking  $\Delta^{-1}$  acting on the above two equalities with the definitions

$$\Delta \psi^{ni} = \phi^{ni} - \bar{\phi}^{ni}, \quad \Delta \psi^n = \phi^n - \bar{\phi}^n, \quad \Delta \psi^{n+1} = \phi^{n+1} - \bar{\phi}^{n+1}$$

leads to

$$\psi^{n+1} = \psi^n + \tau \sum_{i=1}^s b_i \dot{\psi}^{ni}, \quad \psi^{ni} = \psi^n + \tau \sum_{i=1}^s a_{ij} \dot{\psi}^{nj}.$$

We can derive

$$\begin{split} &\frac{\alpha}{2} \left( \|\nabla \psi^{n+1}\|^2 - \|\nabla \psi^n\|^2 \right) \\ &= \frac{\alpha}{2} \left[ \tau \sum_{i=1}^s 2b_i (\nabla \dot{\psi}^{ni}, \nabla \psi^n) + \tau^2 \sum_{i=1}^s \sum_{j=1}^s b_i b_j (\nabla \dot{\psi}^{ni}, \nabla \dot{\psi}^{nj}) \right]. \end{split}$$

Substituting  $\psi^n = \psi^{ni} - \tau \sum_{j=1}^s a_{ij} \dot{\psi}^{nj}$  into the equation above implies

$$\frac{\alpha}{2} \left( \|\nabla \psi^{n+1}\|^2 - \|\nabla \psi^n\|^2 \right)$$

$$= \frac{\alpha}{2} \left[ \tau \sum_{i=1}^s 2b_i (\nabla \dot{\psi}^{ni}, \nabla \psi^{ni}) - \tau^2 \sum_{i=1}^s \sum_{j=1}^s m_{ij} b_i b_j (\nabla \dot{\psi}^{ni}, \nabla \dot{\psi}^{nj}) \right]$$

$$\leq \alpha \tau \sum_{i=1}^s b_i (\nabla \dot{\psi}^{ni}, \nabla \psi^{ni}) = \tau \sum_{i=1}^s b_i (\dot{\phi}^{ni}, \alpha \psi^{ni}). \tag{3.10}$$

Finally, it follows from (3.9) and (3.10) that

$$E(\phi^{n+1}, r^{n+1}) = \frac{\varepsilon^2}{2} \|\nabla \phi^{n+1}\|^2 + \frac{1}{2} |r^{n+1}|^2 + \frac{\alpha}{2} \|\nabla \psi^{n+1}\|^2$$

$$\leq E(\phi^n, r^n) = \frac{\varepsilon^2}{2} \|\nabla \phi^n\|^2 + \frac{1}{2} |r^n|^2 + \frac{\alpha}{2} \|\nabla \psi^n\|^2.$$

**Remark 3.1.** In order construct the linearized scheme (3.4)-(3.6), we can replace  $w(\phi^{ni})$  by  $w(I_{\tau}^{n-1}(\phi^{ni}))$ , where  $I_{\tau}^{n-1}(\phi^{ni})$  is the extrapolation of  $\phi^{ni}$ . The linearized scheme also preserves energy decay in the sense of energy  $E(\phi^n, r^n)$ , the proof can follow the process of the proof of the above theorem.

## 3.4. Fixed-point iteration computation

The system (3.4)-(3.6) is nonlinear if the potential  $f(\phi)$  is nonlinear, which is not easy to compute. One way to deal with this issue is to linearize the system by extrapolation, then solve the linearized equation to obtain the numerical solution. This technique applied to Runge-Kutta scheme for the SAV-reformulated Allen-Cahn and Cahn-Hilliard models is studied in [2]. Linearized system only achieves accuracy of order s instead of p, the reason is that linearization violates the structure of RK method.

In order to solve the nonlinear system (3.4)-(3.6), we adopt fixed-point iteration to compute the nonlinear system directly. It will preserves the structure of RK method and lead to higher accuracy than the extrapolated RK-SAV methods [2].

**Fixed-point iteration.** We solve the nonlinear system directly by fixed-point iteration method. The fixed-point iteration computation for the system (3.4)-(3.6) is constructed as follows:

$$\dot{\phi}^{ni} = M\Delta\varphi^{ni} \qquad \text{in } \Omega, \quad i = 1, \dots, s,$$

$$\phi^{ni} = \phi^{n} + \tau \sum_{j=1}^{s} a_{ij} \dot{\phi}^{nj} \qquad \text{in } \Omega, \quad i = 1, \dots, s,$$

$$\varphi^{ni} = -\varepsilon^{2} \Delta \phi^{ni} + r^{*ni} w (\phi^{*ni}) + \alpha \psi^{*ni} \qquad \text{in } \Omega, \quad i = 1, \dots, s,$$

$$-\Delta \psi^{ni} = \phi^{ni} - \bar{\phi}^{ni} \qquad \text{in } \Omega, \quad i = 1, \dots, s,$$

$$\partial_{n} \phi^{ni} = \partial_{n} \varphi^{ni} = \partial_{n} \psi^{ni} = 0 \qquad \text{or periodic on } \partial \Omega, \quad i = 1, \dots, s,$$

$$\dot{r}^{ni} = \left(w(\phi^{*ni}), \dot{\phi}^{ni}\right), \quad i = 1, \dots, s,$$

$$r^{ni} = r^{n} + \tau \sum_{i=1}^{s} a_{ij} \dot{r}^{ni}, \quad i = 1, \dots, s,$$

$$(3.12)$$

to calculate the numerical solutions  $(\phi^{ni}, r^{ni})$ , i = 1, ..., s on interval temporal nodes until

$$\max \left| \frac{\phi^{ni} - \phi^{\star ni}}{\phi^{ni}} \right| \le \epsilon, \quad \left| \frac{r^{ni} - r^{\star ni}}{r^{ni}} \right| \le \epsilon.$$

Here  $\Box^{*ni}$  denotes numerical solution at previous step in iterating, the initial value can be chosen as  $(\phi^{n-1,i},r^{n-1,i}), i=1,\ldots,s$ , which is close to  $(\phi^{ni},r^{ni}), i=1,\ldots,s$ . For iteration, we can set up a iteration threshold  $\epsilon$  for the difference between  $\Box^{*ni}, \Box^{ni}, i=1,\ldots,s$  for the accuracy of iteration that we desire. Then we can compute  $(\phi^{n+1},r^{n+1})$  with  $(\dot{\phi}^{ni},\dot{r}^{ni}), i=1,\ldots,s$  obtained by Step 1.

Step 2. Computing numerical solutions on temporal nodes

$$\phi^{n+1} = \phi^n + \tau \sum_{i=1}^s b_i \dot{\phi}^{ni},$$

$$r^{n+1} = r^n + \tau \sum_{i=1}^s b_i \dot{r}^{ni}.$$
(3.13)

## 3.5. Full discretization by Fourier-spectral method

We adopt Fourier-spectral method to discretize (3.11)-(3.13) in spatial direction. Without generality we consider this system in interval  $[x_0,x_1]$ . We separate interval into K (even) parts with grids  $1 \le k \le K$ , apply Fourier transform (FT), whose inverse transform is called inverse Fourier transform (IFT), to project the solutions onto function space spanned by the functions  $\{\exp(i2p\pi x/(x_1-x_0)), -K/2 \le p \le K/2-1, p \in \mathbb{Z}\}$ . Denoting by  $\lambda_k$  the coefficients of differential  $\partial_x$  and by  $\hat{\Box}_k$  the transformed functions after FT on each grid k, we have

Step 1. Iterate

$$\hat{\phi}_{k}^{ni} = M \lambda_{k}^{2} \hat{\varphi}_{k}^{ni} \qquad \text{in } \Omega, \quad i = 1, \dots, s,$$

$$\hat{\phi}_{k}^{ni} = \hat{\phi}_{k}^{n} + \tau \sum_{j=1}^{s} a_{ij} \hat{\phi}_{k}^{nj} \qquad \text{in } \Omega, \quad i = 1, \dots, s,$$

$$\hat{\varphi}_{k}^{ni} = -\varepsilon^{2} \lambda_{k}^{2} \hat{\phi}_{k}^{ni} + r \widehat{\psi} \widehat{\psi} \widehat{\psi}^{*ni} + \alpha \hat{\psi}_{k}^{*ni} \qquad \text{in } \Omega, \quad i = 1, \dots, s,$$

$$-\lambda_{k}^{2} \hat{\psi}_{k}^{ni} = \widehat{\phi}^{ni} - \widehat{\phi}_{k}^{ni} \qquad \text{in } \Omega, \quad i = 1, \dots, s,$$

$$\hat{\phi}^{ni} = \text{IFT}(\hat{\phi}^{ni}), \qquad i = 1, \dots, s,$$

$$\hat{\phi}^{ni} = \text{IFT}(\hat{\phi}^{ni}), \qquad i = 1, \dots, s,$$

$$\hat{r}^{ni} = (w(\phi^{*ni}), \hat{\phi}^{ni}), \qquad i = 1, \dots, s,$$

$$r^{ni} = r^{n} + \tau \sum_{i=1}^{s} a_{ij} \hat{r}^{ni}, \quad i = 1, \dots, s,$$

$$(3.15)$$

to compute the numerical solutions on interval temporal nodes until

$$\max_{k} \left\{ \left| \phi_k^{ni} - \phi_k^{\star ni} \right| / \left| \phi_k^{ni} \right| \right\} \leq \epsilon, \quad |r^{ni} - r^{\star ni}| / |r^{ni}| \leq \epsilon.$$

Step 2. Compute numerical solutions on temporal nodes

$$\phi^{n+1} = \phi^n + \tau \sum_{i=1}^s b_i \dot{\phi}^{ni},$$

$$r^{n+1} = r^n + \tau \sum_{i=1}^s b_i \dot{r}^{ni}.$$
(3.16)

It is obvious that we obtain the numerical solutions  $\phi_k^{ni}$ ,  $i=1,\ldots,s$  on interval temporal nodes  $1 \leq k \leq K$  by solving K linear equations of size s in each time-marching iteration, that is to say we can calculate the numerical solutions pointwise on each grid. Our technique substantially reduces the computational requirements. Rather than linearized time-marching schemes, it computes the numerical solution by solving linear system of size  $K \times s$  while it need integrate all unknowns  $\phi_k^{ni}$ ,  $i=1,\ldots,s$  on grids  $k,1\leq k\leq K$ . In higher spatial dimension, such as dim =2,3, the number of grids increases very fast, the computation cost for solving large linear equation will increase rapidly.

If we reformulate PF-BCP model based on IEQ method, then the corresponding constructed fully discretized scheme will have much more stiffness, it will hamper in their performance by stability restrictions. Meanwhile, we need to solve many unknowns as twice as that of the scheme based on SAV method because of the introduced variable is a function over domain  $\Omega$ .

### 4. Numerical Experiments

In this section, we present numerical examples to illustrate the convergence, energy

decay property of the numerical scheme (3.14)-(3.16) for SAV-formulated PF-BCP model. Choosing mean mass adding random perturbed values as the initial values which represents the mixture of two monomer blocks in diblock copolymer, we simulate the evolutions of PF-BCP model. The numerical simulations present the two monomer blocks separate from each other in mixture, which is called phase separation, and we show the effects of various parameter  $\alpha$  on phase separations.

# 4.1. Convergence of RK numerical scheme

In this subsection, we will explore the convergence order by setting the iteration tolerance error to  $\epsilon = 10^{-14}$ . The discussion on the number of iteration steps required for each time step will be given in the next subsection, taking into account the generality of the random initial conditions.

**Example 4.1** (One-Dimensional Case). We consider the following one-dimensional PF-BCP model:

$$\partial_t \phi = M \left[ \Delta (-\varepsilon^2 \Delta \phi + f(\phi)) - \alpha (\phi - \bar{\phi}) \right], \quad (x, t) \in [-0.5, 0.5] \times [0, T]$$

with  $f(\phi) = \phi^3 - \phi$  and initial value  $\phi^0 = \sin^3(2\pi x)$ . The parameters are given by  $\epsilon = 0.01, M = 0.01, T = 1$  and  $\alpha = 0.01$ . We separate the domain [-0.5, 0.5] into  $N_x = 2^7$  sub-domains uniformly. We compute numerical solutions at T = 1 by scheme (3.14)-(3.16) with different temporal stepsize. With  $\tau = 1/2^{16}$  we compute to obtain the numerical solution as the reference solution since the exact solution for the PF-BCP model is unknown. The convergence of numerical computation results are presented in Table 2.

	Stage/Stepsize	$1/2^{8}$	$1/2^9$	$1/2^{10}$	$1/2^{11}$	$1/2^{12}$
Gauss	1	2.03e-05	5.07e-06	1.27e-06	3.16e-07	7.89e-08
			2.00	2.00	2.00	2.00
	2	2.09e-09	1.27e-10	7.90e-12	4.93e-13	3.11e-14
			4.05	4.01	4.00	3.99
Radau IIA	1	1.60e-03	6.33e-04	2.93e-04	1.42e-04	6.82e-05
			1.34	1.11	1.05	1.06
	2	2.46e-07	2.88e-08	3.54e-09	4.40e-10	5.49e-11
			3.09	3.02	3.01	3.00

Table 2: Example 4.1.  $L^2$ -error and convergence order.

Example 4.2 (Two-Dimensional Case). We consider the two-dimensional PF-BCP model

$$\partial_t \phi = M \left[ \Delta (-\varepsilon^2 \Delta \phi + f(\phi)) - \alpha (\phi - \bar{\phi}) \right], \quad (x, y, t) \in [-0.5, 0.5]^2 \times [0, T]$$

with  $f(\phi) = \phi^3 - \phi$  and initial value  $\phi^0 = \sin^3(2\pi x)\sin^3(2\pi y)$ . We choose the parameters M = 0.001,  $\varepsilon = 0.1$ , T = 1 and  $\alpha = 10$  and separate the domain  $[-0.5, 0.5]^2$  into  $2^7 \times 2^7$ 

	Stage/Stepsize	$1/2^{5}$	$1/2^{6}$	$1/2^{7}$	$1/2^{8}$	$1/2^9$
Gauss	1	3.15e-07	7.88e-08	1.97e-08	4.92e-09	1.23e-09
			2.00	2.00	2.00	2.00
	2	1.07e-11	6.69e-13	4.18e-14	2.61e-15	1.63e-16
			4.00	4.00	4.00	3.99
Radau IIA	1	8.28e-05	4.14e-05	2.07e-05	1.03e-05	5.05e-06
			1.00	1.00	1.01	1.02
	2	1.83e-09	2.31e-10	2.89e-11	3.62e-12	4.53e-13
			2.99	2.99	3.00	3.00

Table 3: Example 4.2.  $L^2$ -error and convergence order.

sub-domains uniformly. The reference solution is chosen as the numerical solution computed with temporal stepsize  $\tau=1/2^{15}$ . The numerical computation results with different temporal stepsizes are presented in Table 3.

Tables 2 and 3 show that the  $L^2$ -error of the RK scheme (3.14)-(3.16) achieves accuracy of order p=2s and p=2s-1 based on s-stage Gauss method and Radua IIA method respectively. Under the stability condition of algebraically stable RK methods, the numerical scheme (3.14)-(3.16) preserves the energy decay property of PF-BCP model. The energy decay versus t for the PF-BCP model in one-dimensional and two-dimensional cases are plotted in Fig. 1 (left) and (right) respectively.

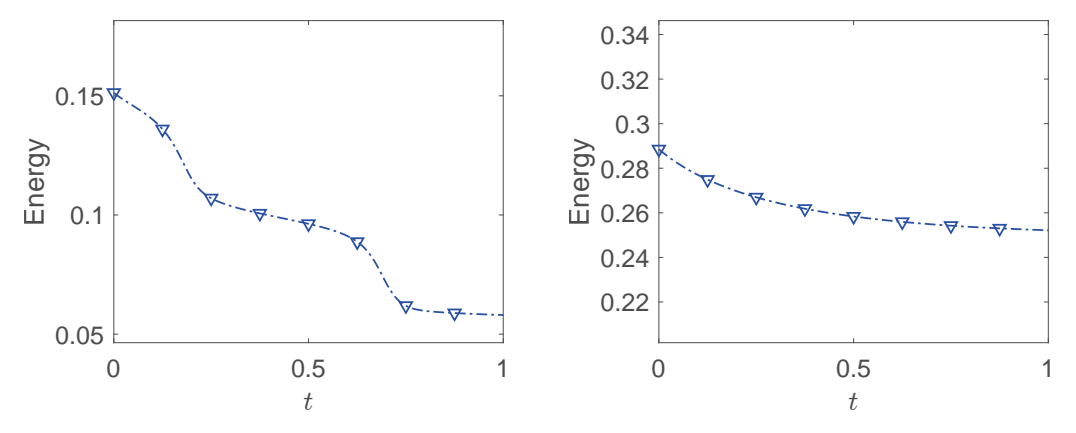


Figure 1: Evolution of the energy. Left: Example 4.1. Right: Example 4.2.

## 4.2. Phase separations in two-dimensional domain

In this section, we study the phase separation of PF-BCP model in two-dimensional domain. The phase separation describes the molecular self-assembly monomer blocks of DC model to form lamellar or cylindrical nanostructures through two monomer blocks separating from the mixture.

In the PF-BCP model, the phase separation manifests in the spontaneous growth of the concentration fluctuations that leads the system from homogeneous state to the separated two-phase state. There are specified interface forming between them, 1 and -1 represents pure monomer blocks A and B respectively. After the phase separation starts, the domains of two phase states are formed in short time and the infinitesimal interface between two states are specified and deforming.

We choose initial condition as random perturbed concentration field which is referred to as mixture of two-state monomer blocks as follows:

$$\phi(x, y, 0) = \hat{\phi}_0 + 0.01 \times \text{rand}(x, y), \quad (x, y) \in [-0.5, 0.5]^2,$$

where the function  $\operatorname{rand}(x,y)$  denotes the uniformly distributed random function valued in [0,1].  $\hat{\phi}_0$  can be viewed as the mean value of the phase field due to the small perturbation, which determines evolving the phase field into lamellar or cylindrical structure with different values chosen.

Next, we will present some numerical simulations of PF-BCP model by numerical scheme (3.14)-(3.16) with different initial conditions and parameters  $\alpha$  to study the structure of phase field and the effect of one-order linking two distinct monomer blocks on phase separations.

**Example 4.3** (Lamellar-Structured PF-BCP). Firstly, we set up parameters as M=0.01,  $\varepsilon=0.01$  in the PF-BCP model. Next, we will investigate the effects of parameter  $\alpha$  on the coarsening dynamics. We consider the lamellar-structured phase field, choosing  $\hat{\phi}_0=0$ . On spatial dimension, we separate the domain  $[-0.5,0.5]^2$  into  $2^7\times 2^7$  sub-domains uniformly. We simulate the PF-BCP model by our Gauss RK algorithm with stage s=2. The numerical profiles of  $\phi$  at t=0,0.002,0.005,0.01,0.1,0.5,1,2 are summarized in Figs. 2-4 with temporal stepsize  $\tau=5\times 10^{-5}$ . Time evolution of the energy decay versus t for the diblock-copolymer model with  $\hat{\phi}_0=0$  and  $\alpha=0.001,10,100$  is plotted in Fig. 5.

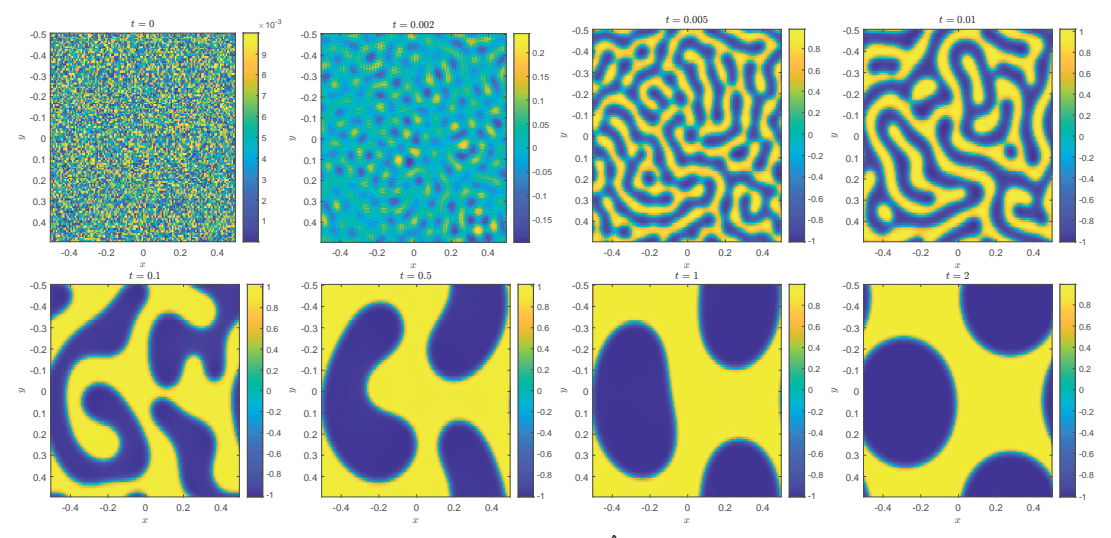


Figure 2: Example 4.3. PF-BCP model,  $\alpha = 0.001$ ,  $\hat{\phi}_0 = 0$ , t = 0, 0.002, 0.005, 0.01, 0.1, 0.5, 1, 2.

Figs. 2-4 show that the phase field keeps evolving into the separated parts of monomer blocks A, valued 1 (yellow) and monomer blocks B, valued -1 (blue) as t increasing until the phase field becomes stable state. In the phase separation, the phase field evolves into lamellar structure. The evolution of the PF-BCP model behaves like Cahn-Hilliard model when the parameter  $\alpha$  is small. Meanwhile, the phase field becomes stable as faster as parameter  $\alpha$  larger, which verifies that the nonlocal term represents the first-order effect of the connectivity between the two monomer blocks.

It can be obviously seen from the Fig. 5 (left) that the energy of PF-BCP model decays to the stable state earlier as  $\alpha$  increasing and the energy in stable state is larger as  $\alpha$  increasing.

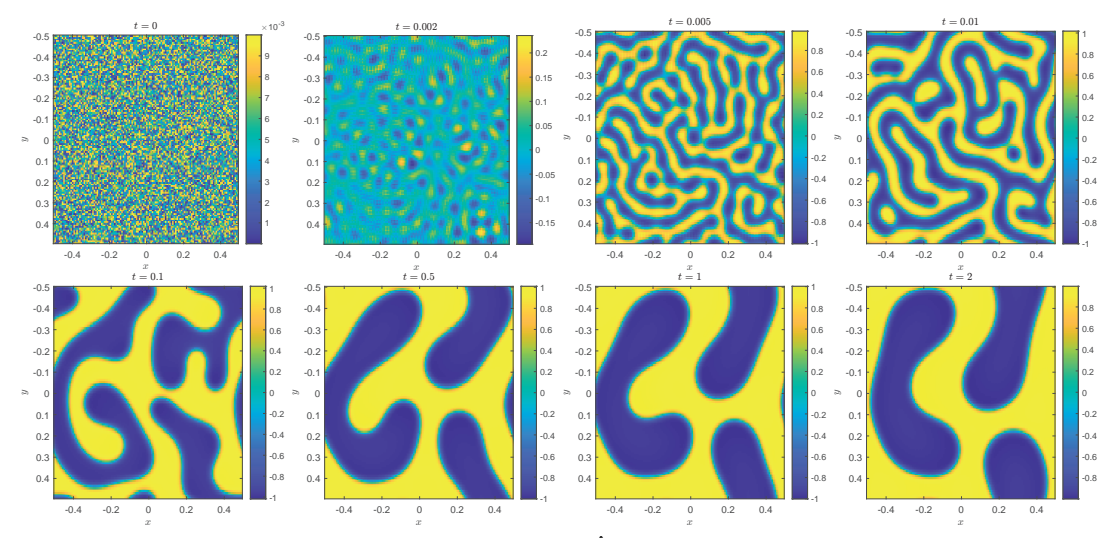


Figure 3: Example 4.3. PF-BCP model,  $\alpha = 10$ ,  $\hat{\phi}_0 = 0$ , t = 0, 0.002, 0.005, 0.01, 0.1, 0.5, 1, 2.

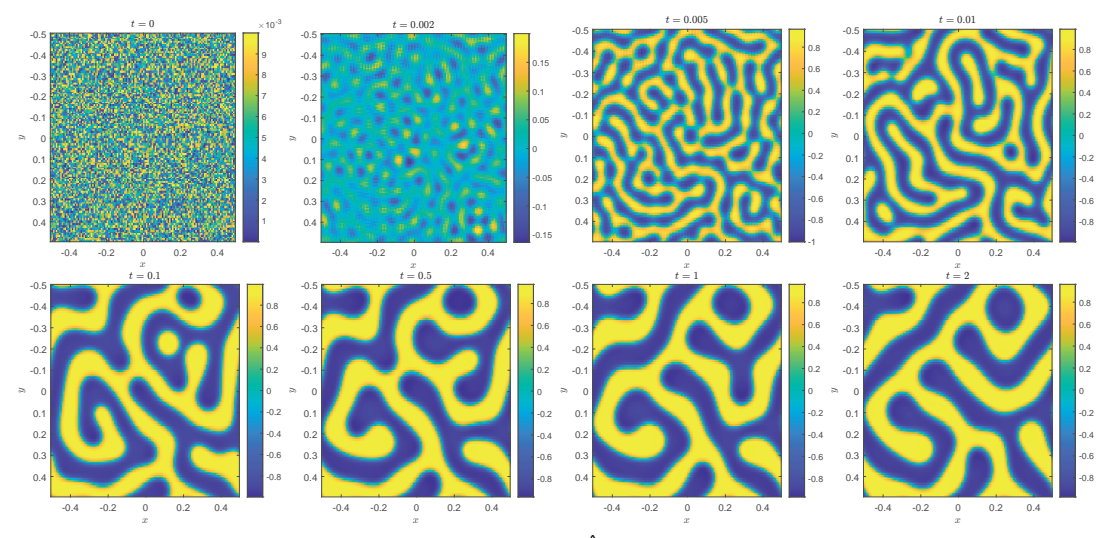


Figure 4: Example 4.3. PF-BCP model,  $\alpha = 100$ ,  $\hat{\phi}_0 = 0$  at t = 0, 0.002, 0.005, 0.01, 0.1, 0.5, 1, 2.

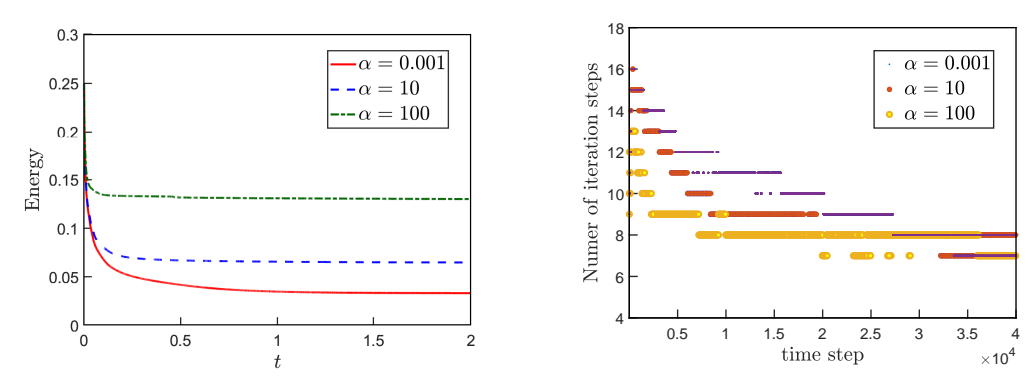


Figure 5: Example 4.3. Left: Time evolution of energy decay versus t for diblock-copolymer model,  $\hat{\phi}_0 = 0$ ,  $\alpha = 0.001, 10, 100$ . Right: Number of iteration steps required for each time step.

From this, it can be inferred that the nonlocal term  $\alpha(\phi - \bar{\phi})$  in PF-BCP model strengthens the connectivity of two monomer blocks which verifies the one-order linking effect of the nonlocal term. We select a convergence criterion  $\epsilon$  equal to  $10^{-8}$ . We trick the number of iteration steps necessary for each time step, and the corresponding data is presented in the right side of Fig. 5. It indicate that the iteration steps consistently require a similar number of iterations to attain the desired precision  $\epsilon$ .

**Example 4.4** (Cylindrical-Structured PF-BCP). Furthermore, we simulate the phase separations of the PF-BCP model with initial condition  $\hat{\phi}_0 = 0.3$  to produce cylindrical-structured phase field. The numerical profiles of  $\phi$  at t = 0,0.002,0.005,0.01,0.1,0.5,1,2 are summarized in Figs. 6-8 with temporal stepsize  $\tau = 5 \times 10^{-5}$ . We plot the time evolution of the energy decay versus t for the PF-BCP model with  $\hat{\phi}_0 = 0.3$  and  $\alpha = 0.001,10,100$  in Fig. 9.

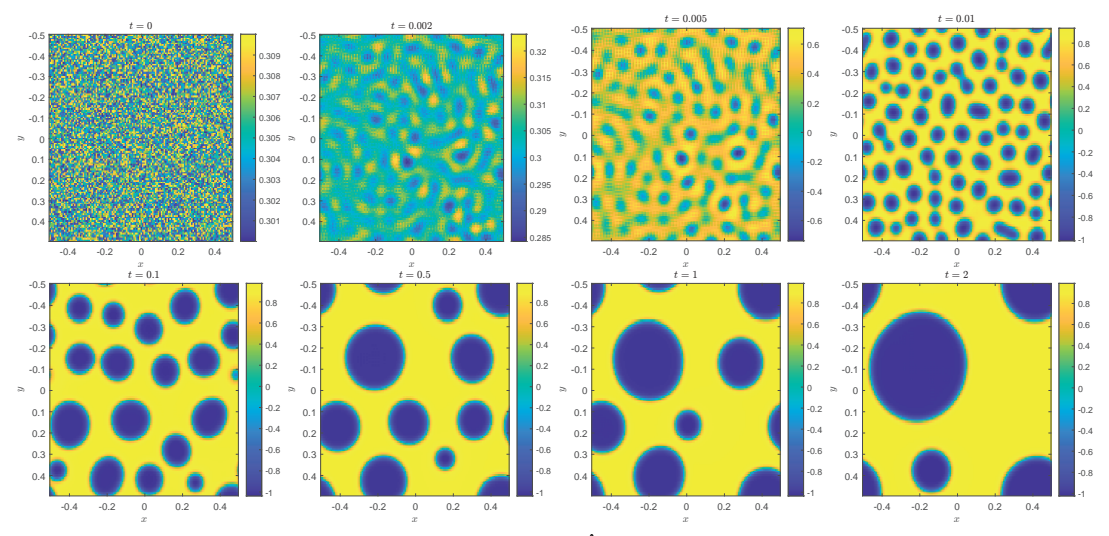


Figure 6: Example 4.4. PF-BCP model,  $\alpha = 0.001$ ,  $\hat{\phi}_0 = 0.3$  at t = 0, 0.002, 0.005, 0.01, 0.1, 0.5, 1, 2.

Due to the mean value of the mass of phase field  $\hat{\phi}_0=0.3$  is positive, the phase of the PF-BCP model in Figs. 6-8 evolves into cylindrical structures, which means monomer A blocks (state 1) dominates in the domain  $\Omega$ , state -1 part will evolve into cylindrical structure via phase separation. If the mean value  $\hat{\phi}_0=0$ , then two monomer blocks do not dominate in the domain either, hence the phase field will evolve into lamellar structure, which is confirmed in Figs. 2-4 with  $\hat{\phi}_0=0$ . Also, the simulations of cylindrical-structured phase field with different  $\alpha$  verify that the nonlocal term represents the first-order effect of the connectivity between the two monomer blocks.

From Fig. 9 (left), we can see that the time evolutions of the energy decay of PF-BCP model with various  $\alpha = 0.001, 10, 100$  are almost similar to Fig. 5 which choose initial

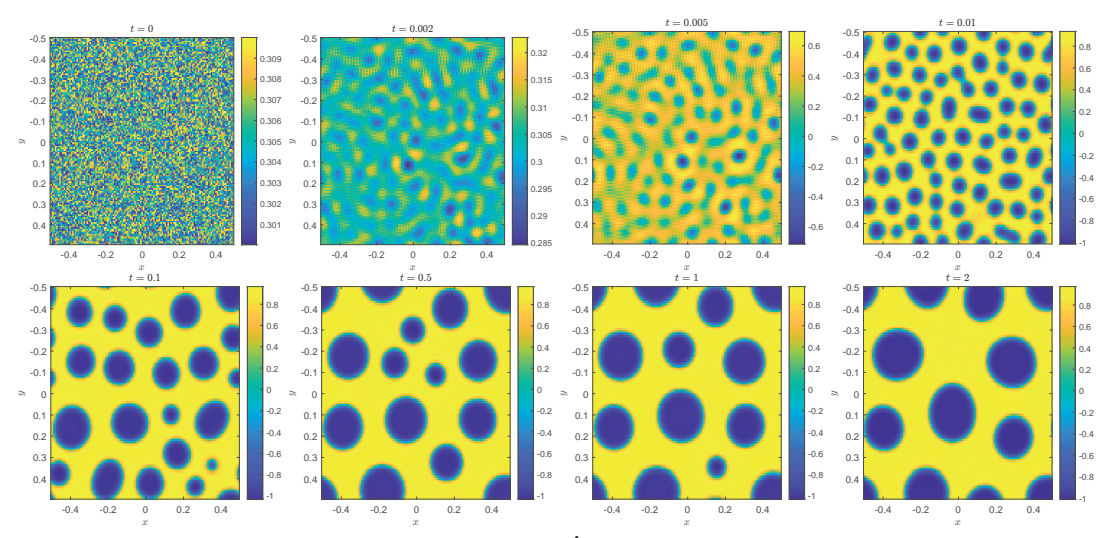


Figure 7: Example 4.4. PF-BCP model,  $\alpha = 10$ ,  $\hat{\phi}_0 = 0.3$  at t = 0, 0.002, 0.005, 0.01, 0.1, 0.5, 1, 2.

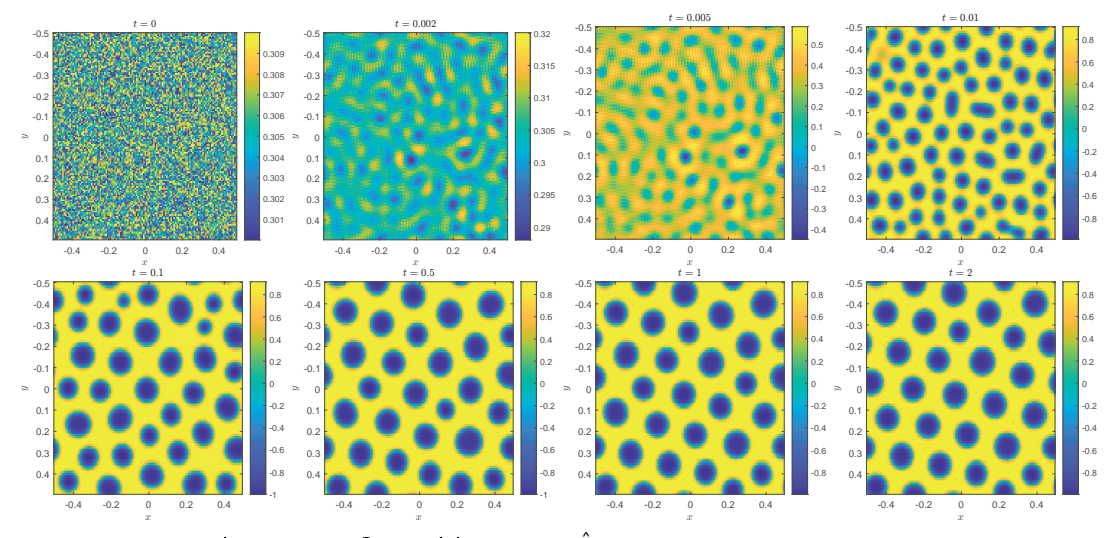


Figure 8: Example 4.4. PF-BCP model,  $\alpha = 100$ ,  $\hat{\phi}_0 = 0.3$  at t = 0, 0.002, 0.005, 0.01, 0.1, 0.5, 1, 2.

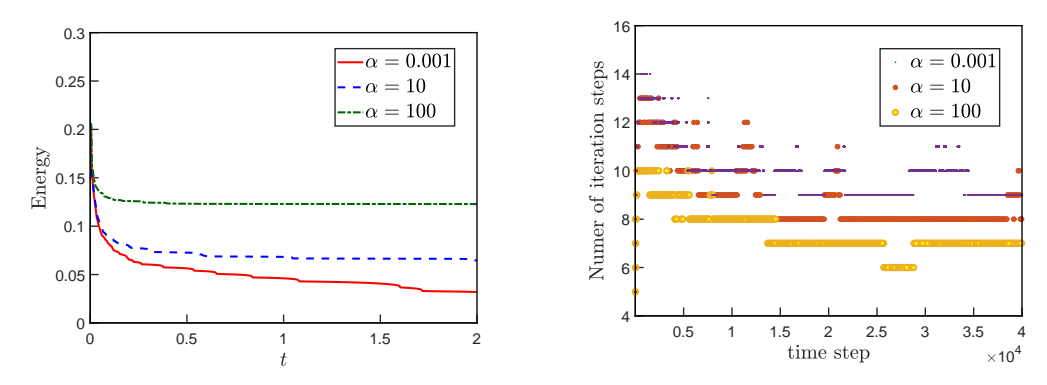


Figure 9: Example 4.4. Left: Time evolution of energy decay versus t for diblock-copolymer model,  $\hat{\phi}_0 = 0.3$ ,  $\alpha = 0.001, 10, 100$ . Right: Number of iteration steps required for each time step.

condition as  $\hat{\phi}_0 = 0$ . By setting iteration tolerance error  $\epsilon$  to  $10^{-8}$ , we observe that the number of iteration steps is nearly identical to the previous simulation, see the Fig. 9 (right).

#### 5. Conclusion

Diblock copolymers are copolymers composed of two monomer blocks of fluid-like disorder, which forms free interfaces in the evolution. In Lagrangian framework, it is difficult to describe diblock copolymers due to free interfaces. In order to describe a system with free interfaces efficiently, the PF-BCP model is introduced to deal with the difficulty in matching boundary conditions on the interfaces between two blocks of copolymer in Eulerian framework.

In this paper, we reformulate the PF-BCP model based on SAV method, then construct energy stable time-marching scheme by adopting algebraically stable RK methods. The nonlinear system is solved by fixed-point iteration method. The energy decay is proved rigorously. The Fourier-spectral method is adopted to discretize on the spatial dimension. We can compute numerical solutions pointwise on each grid, hence proposed algorithm reduces computational requirements.

The high-accuracy and energy decay property are verified by the numerical examples. The phase separation simulations confirm the efficiency of our algorithm for the PF-BCP model. Finally, we discussed the influence on the evolutions about the initial conditions and parameters  $\alpha$ .

## Acknowledgments

The authors would like to thank Dr. Zongze Yang for valuable discussions, which helped to improve the quality of the paper.

L.Ch. would like to acknowledge the support of the National Natural Science Foundation of China (Grant Nos. 12131005, U2230402). The work of B.R. was partially supported

by the National Natural Science Foundation of China (Grant Nos. 12071020, 12131005, U2230402).

#### References

- [1] A.C. Aristotelous, O. Karakashian and S.M. Wise, *A mixed discontinuous Galerkin, convex splitting scheme for a modified Cahn-Hilliard equation and an efficient nonlinear multigrid solver*, Discrete Contin. Dyn. Syst. B **18(9)**, 2211–2238 (2013).
- [2] G. Akrivis, B. Li and D. Li, Energy-decaying extrapolated RK-SAV methods for the Allen-Cahn and Cahn-Hilliard equations, SIAM J. Sci. Comput. **41(6)**, A3703–A3727 (2019).
- [3] F. Boyer and S. Minjeaud, *Numerical schemes for a three component Cahn-Hilliard model*, ESAIM: Math. Model. Numer. Anal. **45(4)**, 697–738 (2011).
- [4] R. Choksi, M.A. Peletier and J.F. Williams, On the phase diagram for microphase separation of diblock copolymers: An approach via a nonlocal Cahn-Hilliard functional, SIAM J. Appl. Math. **69(6)**, 1712–1738 (2009).
- [5] D.J. Eyre, An unconditionally stable one-step scheme for gradient systems (1997). https://citeseerx.ist.psu.edu/document?repid=rep1&type=pdf&doi=4f016a98fe25bfc06b9bcab3d85eeaa47d3ad3ca
- [6] J.J. Feng, C. Liu, J. Shen and P. Yue, An energetic variational formulation with phase field methods for interfacial dynamics of complex fluids: Advantages and challenges, in: Modeling of Soft Matter. The IMA Volumes in Mathematics and its Applications, M.T. Caldererpp and E.M. Terentjev (Eds), pp. 1–26, Springer (2005).
- [7] D. Jeong, J. Shin, Y. Li, Y. Choi, J. Jung, S. Lee and J. Kim, *Numerical analysis of energy-minimizing wavelengths of equilibrium states for diblock copolymers*, Curr. Appl. Phys. **14(9)**, 1263–1272 (2014).
- [8] X. Feng and A. Prohl, Numerical analysis of the Allen-Cahn equation and approximation for mean curvature flows, Numer. Math. 94, 33–65 (2003).
- [9] Y. Gong and J. Zhao, Energy-stable Runge-Kutta schemes for gradient flow models using the energy quadratization approach, Appl. Math. Lett. **94**, 224–231 (2019).
- [10] F. Huang, J. Shen and Z. Yang, *A highly efficient and accurate new scalar auxiliary variable approach for gradient flows*, SIAM J. Sci. Comput. **42(4)**, A2514–A2536 (2020).
- [11] Y. Peng, Y. Lu, Z. Chen and G. Yu, A binary phase field crystal study for phase segregation of liquid phase heteroepitaxial growth, Comput. Mater. Sci. 123, 65–69 (2016).
- [12] G. Tegze, G. Bansel, G.I. Tóth, T. Pusztai, Z. Fan and L. Gránásy, Advanced operator splitting-based semi-implicit spectral method to solve the binary phase-field crystal equations with variable coefficients, J. Comput. Phys. 228(5), 1612–1623 (2009).
- [13] J. Shen and J. Xu, Convergence and error analysis for the scalar auxiliary variable (SAV) schemes to gradient flows, SIAM J. Numer. Anal. **56**, 2895–2912 (2018).
- [14] J. Shen, J. Xu and J. Yang, *The scalar auxiliary variable (SAV) approach for gradient flows*, J. Comput. Phys. **353**, 407–416 (2018).
- [15] J. Shen and X. Yang, Numerical approximations of Allen-Cahn and Cahn-Hilliard equations, Discrete Contin. Dyn. Syst. **28(4)**, 1669–1691 (2010).
- [16] G. Wanner and E. Hairer, Solving Ordinary Differential Equations II: Stiff and Differential-Algebraic Problems, Springer Series in Computational Mathematics 14, Springer (1996).
- [17] X. Wu and Y.A. Dzenis, *Phase-field modeling of the formation of lamellar nanostructures in diblock copolymer thin films under inplanar electric fields*, Phys. Rev. E **77(3)**, 031807 (2008).
- [18] X. Yang and G. Zhang, Convergence analysis for the invariant energy quadratization (IEQ) schemes for solving the Cahn-Hilliard and Allen-Cahn equations with general nonlinear potential,

- J. Sci. Comput. 82, 1-28 (2020).
- [19] Y. Zhang and J. Shen, A generalized SAV approach with relaxation for dissipative systems, J. Comput. Phys. **464**, 111311 (2022).
- [20] J. Zhao, X. Yang, Y. Gong and Q. Wang, A novel linear second order unconditionally energy stable scheme for a hydrodynamic q-tensor model of liquid crystals, Comput. Methods Appl. Mech. Eng. 318, 803–825 (2017).